Journal of Power Sources 196 (2011) 2445–2451

Contents lists available at ScienceDirect

Journal of Power Sources

journal homepage: www.elsevier.com/locate/jpowsour

Review

Dependence of open-circuit potential and power density on electrolyte thickness in solid oxide fuel cells with mixed conducting electrolytes

Keith L. Duncan[a], Kang-Taek Lee[a], Eric D. Wachsman[b,*]

[a] Department of Materials Science and Engineering, University of Florida, Gainesville, FL 32611-6400, USA
[b] University of Maryland Energy Research Center, University of Maryland, College Park, MD 20742-2115, USA

ARTICLE INFO

Article history:
Received 6 August 2010
Received in revised form 8 October 2010
Accepted 12 October 2010
Available online 20 October 2010

Keywords:
Solid oxide fuel cell (SOFC)
Modeling
Mixed conducting electrolyte or mixed ionic-electronic conductor (MIEC)
Electrolyte open circuit voltage/potential (OCV or OCP)
Power density
Ceria

ABSTRACT

A continuum-level electrochemical model previously developed by the authors [1] is used to investigate the dependence of open-circuit voltage (OCV), and maximum power density on electrolyte thickness for solid oxide fuel cells (SOFCs) with mixed conducting electrolytes. Experimental results confirm the models predictions that OCV decreases monotonically with decreasing electrolyte thickness due to increased permeation flux [1]. The model was further extended to show that there exists an optimal electrolyte thickness at which maximum power density occurs for mixed conducting electrolytes. As expected, for electrolyte thickness greater than optimal losses from ohmic overpotential reduce cell output. However, when the electrolyte thickness is lower than optimal losses from an increasing electronic "leakage" current reduce cell output.

Contents

1. Introduction

Acceptor-doped ceria has widely been investigated as an electrolyte in solid oxide fuel cells (SOFCs), especially at intermediate temperatures (500–700 °C) [1–7]. However, although acceptor-doped ceria has excellent ionic conductivity (up to 5 times higher than yttria-stabilized zirconia, YSZ [5–7]) it is a mixed conductor—i.e., it conducts electrons in addition to oxygen ions—in typical SOFC operating conditions [5,6]. This results in a deleterious leakage current during operation that reduces overall SOFC efficiency [2–6]. This leakage current, as a fraction of total current, increases as the cell voltage increases and in open-circuit conditions its effect shows up as a reduction in the open-circuit voltage from the theoretical (Nernst) value.

* Corresponding author. Tel.: +1 301 405 8193; fax: +1 301 314 8514.
E-mail address: ewach@umd.edu (E.D. Wachsman).

0378-7753/$ – see front matter © 2010 Elsevier B.V. All rights reserved.
doi:10.1016/j.jpowsour.2010.10.034

Recent studies have shown that electrolyte thickness is also a factor in the magnitude of the leakage current and, therefore, the open circuit voltage [1,8]. Indeed, it was shown experimentally [8] and theoretically [1] that reducing electrolyte thickness also reduced open-circuit voltage. However, open-circuit voltage is a marker for the maximum potential energy available to an SOFC. Hence for SOFCs with mixed conducting electrolytes the typical approach of making ever thinner electrolytes to increase maximum current density (by reducing ohmic losses) may not be applicable to MIEC electrolytes. In other words, for mixed conducting electrolytes there is likely a trade-off between reducing ohmic losses and maintaining a high enough open-circuit potential. Consequently, one may reasonably infer that there exists a optimum thickness at which maximum power density is attained. SOFC electrolytes with a thickness below the optimum value have a reduced power density because of too great a loss in available potential energy, i.e., too low an open-circuit voltage. Similarly, SOFC electrolytes with a thickness above the optimum value also have a reduced power density, but now because of increased ohmic losses.

In addition, a survey of the literature shows great inconsistency in the open-circuit voltages (OCVs) reported by various groups for SOFCs with acceptor-doped ceria electrolytes, even with electrolytes of similar thickness [1–7]. While the inconsistency in OCVs could be attributable in part to differences in GDC film quality (due to variations in porosity, homogeneity, etc.), they are nevertheless, particularly stark when contrasted to the absence of similar variation for SOFCs with YSZ electrolytes (which have similar issues with film quality). Since YSZ is a purely ionic conductor, one may deduce that the variability seen in SOFCs with acceptor-doped ceria electrolytes is also a consequence of mixed conductivity therein.

As a corollary of the authors' previous work on modeling of SOFC electrochemical performance [1], this paper explores the hypothesis introduced above by modeling the performance of real SOFCs from our laboratory and elsewhere in an effort to deduce the optimal thickness of acceptor-doped ceria electrolytes and to properly describe all the factors that play a role in measured open-circuit voltages of SOFCs with acceptor-doped ceria electrolytes.

2. Theory

A general model for SOFC performance in all operating conditions was derived in entirety in our earlier work [1]. Modeling the dependence of open-circuit voltage, Φ_{oc}, on thickness and electrode characteristics is a subset of that work and so, in this section, only the relevant features are summarized.

2.1. Current–voltage relationships

The equivalent circuit of an SOFC, of thickness L, is shown in Fig. 1, where oxygen partial pressure, $P_{O_2,0}$ (at $x = 0$, i.e., the anode side) and $P_{O_2,L}$ (at $x = L$, i.e., the cathode side) are the P_{O_2}'s on either side of the MIEC. Fig. 1 shows the most widely reported SOFC conventional equivalent circuit in the literature [9–16]. Circuit analysis shows, given $\eta = \eta_0 + \eta_L$, that

$$J = J_v + J_e = (\Phi_{th} - \eta - \Phi_{ext})R_v^{-1} - \Phi_{ext}R_e^{-1} \quad (1)$$

where η is the total interfacial activation overpotential, η_0 is the activation overpotential at the anode-electrolyte interface, η_L is the activation overpotential at the cathode-electrolyte interface, J is current density drawn by the load (i.e., external circuit), Φ_{ext} is the potential difference across a load or applied by an external source, Φ_{th} is the theoretical/Nernst voltage and R is electrical resistance. Additionally, the subscripts "0" and "L" refer to the anode/reducing side (i.e., at $x = 0$) and the cathode/oxidizing side (i.e., at $x = L$) of the electrolyte, respectively (as shown in Fig. 1); while the subscripts "v" and "e" refer to oxygen vacancies (i.e., the mobile ionic species) and electrons, respectively. Fig. 1 and Eq. (1) both show that at open circuit ($J = 0$) $J_v = J_e \neq 0$ and $\Phi_{oc} = (\Phi_{th} - \eta - \Phi_{ext})R_eR_v^{-1}$ Therefore, since R_e and R_v are both functions of thickness, it is clear that Φ_{oc} will be as well.

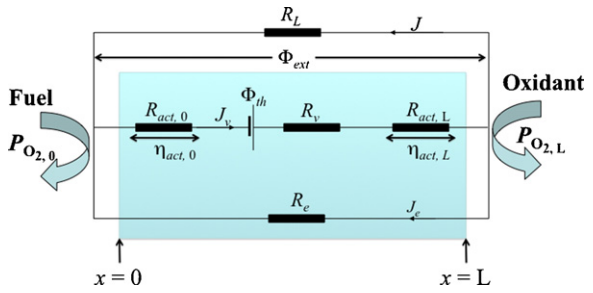

Fig. 1. Equivalent circuit of an SOFC. Φ_{th} represents the theoretical or Nernst voltage. The cell output voltage, Φ_{ext}, is applied to a load resistance, R_L, through which flows the cell output current, J, electronic 'leakage' current, J_e, flows through the electronic resistance, R_e, while the cell activation overpotentional is represented by $R_{act,0}$ and $R_{act,L}$ for the anode and cathode, respectively. The ionic current J_v is greater than J and flows through the ionic resistance R_v.

2.2. Thermodynamics

For dilute concentrations of point defects (i.e., where the electrochemical potential of lattice oxygen $\tilde{\mu}_{O_O^\times}$ is approximately constant), the oxygen exchange reaction between the MIEC and the gas phase is given (in Kröger-Vink notation) by

$$O_O^\times \leftrightarrow V_O^{\bullet\bullet} + 2e' + \frac{1}{2}O_2, \quad K = c_v c_e^2 P_{O_2}^{1/2} \quad (2)$$

where K is the mass action (equilibrium) constant for the reaction and c is concentration.

At the anode interface, the reaction in Eq. (2) proceeds to the right, while at the cathode interface it proceeds to the left. Accordingly, it was shown in our earlier work [1] that

$$K_0 = K^* \exp(-2qk_B^{-1}T^{-1}\eta_0) = c_{v,0}c_{e,0}^2 P_{O_2,0}^{1/2} \quad (3)$$

$$K_L = K^* \exp(2qk_B^{-1}T^{-1}\eta_L) = c_{v,L}c_{e,L}^2 P_{O_2,L}^{1/2} \quad (4)$$

where K_0 and K_L are the equilibrium constant for oxygen exchange at the anode–electrolyte interface and cathode–electrolyte interfaces, respectively, and is the equilibrium constant for K^* oxygen exchange when $\eta_0 = \eta_L = 0$; also T is temperature, q is elementary electron charge and k_B is Boltzmann's constant. Eqs. (3) and (4) show that K is affected by the overpotential at the electrode, i.e., the amount of oxygen incorporated (cathode) in or released (anode) by the electrolyte is a function of the electrode overpotential. Consequently, through Eq. (2), the concentration of defect species at the boundaries (i.e., at $x = 0$ and $x = L$) is dependent on potential. It is noted here that defect formation in electrode materials is excluded because it primarily affects electrode kinetics which is discussed in the following section.

2.3. Kinetics

The transport model derived in the next section must be related to the kinetics of electron transfer at the electrodes. This is done through the Butler-Volmer equation, which may be approximated as follows [17,18]

$$J_v = 2J_{ex,0}\sinh(2^{-1}qk_B^{-1}T^{-1}\eta_0) \quad \text{relative to the anode} \quad (5)$$

or

$$J_v = 2J_{ex,L}\sinh(2^{-1}qk_B^{-1}T^{-1}\eta_L) \quad \text{relative to the cathode} \quad (6)$$

where J_{ex} is the exchange current density. In the Butler-Volmer equation, J_{ex} encapsulates the material properties of an electrode that determine its performance in the SOFC.

Moreover, if α is defined as the ratio of the anodic exchange current density to the cathodic exchange current density (i.e., $\alpha = J_{ex,0}/J_{ex,L}$), then combining Eqs. (5) and (6) yields

$$\eta_L = 2q^{-1}k_BT\ \sinh^{-1}\left(\alpha\ \sinh\left(\frac{1}{2}qk_B^{-1}T^{-1}\eta_0\right)\right) \tag{7}$$

i.e., the cathodic overpotential is a function of the anodic overpotential and vice versa.

This approach is a significant departure from existing models [9–16] in which the distinctions between the individual characteristics (as determined by their material properties) of the anode versus the cathode are ignored. Specifically, the Butler-Volmer equation is employed in such a way that only η is reported (i.e., the distinct contributions of η_0 and η_L are ignored) and J_{ex} is representative of the effective exchange current density of both electrodes combined. Arguably, this practice may be acceptable for ideally reversible electrodes, but for real, irreversible electrodes more sophistication is desirable. In the proposed approach outlined above, it is possible, in principle, to separate η into η_0 and η_L, and obtain $J_{ex,0}$ and $J_{ex,L}$. We hasten to point out, however, that this approach can only provide *apparent* values for η_0 and η_L, and thereby $J_{ex,0}$ and $J_{ex,L}$, since the absolute measurement of η_0 and η_L requires the use of a suitable reference electrode [17–20]. Nevertheless, the *apparent* values obtained for η_0 and η_L, and thereby $J_{ex,0}$ and $J_{ex,L}$, will provide much needed insight into the performance characteristics of SOFCs.

2.4. Physical significance

The crucial feature of the thermodynamic and kinetic equations developed above is the occurrence of η in each of the equation sets: Eqs. (3) and (4) (thermodynamics) and Eqs. (5)–(7) (kinetics). For mixed-conducting electrolytes this is fundamental, because it shows how electrode properties influence the thermodynamics (i.e., the defect populations) of the electrolyte (and vice versa). This becomes clear after substituting Eqs. (5) and (6) into Eqs. (3) and (4), respectively, as shown below

$$K_0 = K^*\ \exp\left(-4\ \sinh^{-1}\left(\frac{1}{2}\frac{J_v}{J_{ex,0}}\right)\right) = c_{v,0}c_{e,0}^2P_{O_2,0}^{1/2} \tag{8}$$

$$K_L = K^*\ \exp\left(4\ \sinh^{-1}\left(\frac{1}{2}\frac{J_v}{J_{ex,L}}\right)\right) = c_{v,L}c_{e,L}^2P_{O_2,L}^{1/2} \tag{9}$$

Consequently, as will demonstrated later, this approach allows the characteristics of any type of electrode to be correctly incorporated into the SOFC performance model developed herein.

The effect is clearly seen in Φ_{oc} measurements reported for SOFCs with mixed conducting electrolytes such as acceptor-doped ceria. In open-circuit conditions with mixed conducting electrolytes, $J = 0$ but $J_v \neq 0$ hence $\eta \neq 0$. Therefore, as Eqs. (8) and (9) show, the defect populations (as well as K_0 and K_L) are dependent on $J_{ex,0}$ and $J_{ex,L}$ even at open-circuit. In other words, with a mixed conducting electrolyte, Φ_{oc} depends on the electrodes employed. This result is supported by the literature [21–23] where (for the same T, $P_{O_2,0}$ and $P_{O_2,L}$) there is an appreciable variance in Φ_{oc} reported for SOFCs with acceptor-doped ceria electrolytes which is largely due to the electrodes used, Fig. 1. In contrast, for SOFCs with YSZ electrolytes the variance in reported Φ_{oc} is negligible since, for purely ionic conducting electrolytes like YSZ, $J = J_v = 0$ and $\eta = 0$.

2.5. Open circuit voltage

In open circuit conditions, there is no current drawn by an external circuit so that $J = 0$. From the authors' earlier work [1], the following expressions for Φ_{oc} and the open-circuit oxygen vacancy current, $J_{v,oc}$, were derived,

$$\Phi_{oc} = \Phi_{th} - \eta_{oc} - \frac{k_BT}{q}\left(\frac{1}{z_v}\ln\frac{c_{v,0}}{c_{v,L}} + \frac{D_e - D_v}{z_vD_v - z_eD_e}\ln\frac{z_v(u_e-u_v)c_{v,0} - u_ec_a}{z_v(u_e-u_v)c_{v,L} - u_ec_a}\right) \tag{10}$$

$$L = \frac{u_vu_eq\lambda\gamma_{oc}c_a}{2(u_v-u_e)J_{ex,0}}\left[\sinh\left(\frac{q}{2k_BT}\eta_{0,oc}\right)\right]^{-1} \tag{11}$$

$$J_{v,oc} = \frac{q\lambda\gamma_{oc}u_vu_ec_a}{(u_v-u_e)L} = 2J_{ex,0}\ \sinh\left(\frac{q}{2k_BT}\eta_{0,oc}\right) \tag{12}$$

given

$$\lambda = k_BTq^{-1}c_a^{-1}\frac{z_v - z_e}{z_e} \quad \text{and}$$

$$\gamma_{oc} = \frac{1}{\lambda}\left(\Phi_{oc} + \eta_{oc} - \Phi_{th} - \frac{k_BT}{z_Vq}\ln\frac{c_{v,L}}{c_{v,0}}\right) - (c_{v,L} - c_{v,0}) \tag{13}$$

where L is electrolyte thickness, z is charge number ($z_e = -1$ and $z_v = 2$), D is diffusivity, u is mobility and c_a is acceptor dopant concentration—preset by material synthesis and for the case study material, ceria (CeO_2) the acceptor dopant of choice is trivalent Gd^{3+} or Sm^{3+}.

Eqs. (10) and (11) are a set of parameterized equations in terms of $\eta_{0,oc}$. Hence the dependence of Φ_{oc} on L can be educed by first obtaining the $\Phi_{oc}(\eta_{0,oc})$ and $L(\eta_{0,oc})$. This was done with $J_{ex,0}$ and $J_{ex,L}$ as the only fitting parameters.

2.6. Maximum power density

Electrolyte thickness also plays a role in maximum power density. In pure ionic conducting electrolyte, the maximum power density increases monotonically with decreasing electrolyte thickness. However, for mixed conducting electrolytes (due to the higher mobility of the electronic species), it is possible that the magnitude of the leakage current increases with decreasing thickness faster than the ionic current. Therefore, with mixed conducting electrolytes, the SOFC output power can end up eventually decreasing as the electrolyte thickness decreases. This phenomenon can be explored by plotting the maximum power density as a function of thickness using the equation below [1]:

$$P_{load} = \Phi_{ext}^*J = J\left(\Phi_{th} - \eta_{act} - R_{elec} + \frac{k_BT}{z_Vq}\ln\frac{c_{v,L}}{c_{v,0}}\right) + \frac{z_v(D_e - D_v)\gamma + (J/q)}{z_v(u_v-u_e)(\gamma/JL)}\ln\frac{z_v(u_e-u_v)c_{v,L} - u_ec_a - (JL/q\lambda\gamma)}{z_v(u_e-u_v)c_{v,0} - u_ec_a - (JL/q\lambda\gamma)} \tag{14}$$

where R_{elec} is the sum of the non-electrolyte ohmic resistances, including the resistances of the leads, the current collectors and the electrodes as well as contact resistances; Φ_{ext}^* is therefore the corrected external potential.

As detailed by Duncan and Wachsman [1], Eq. (14) can be used to obtain the current–voltage and current–power curves a fuel cell of a given electrolyte thickness. Consequently, after fitting the model to experimental data for a given electrolyte thickness, the maximum power density can be predicted for other electrolyte thicknesses (assuming concentration overpotential is negligible).

3. Experimental

To validate the models described above a series of anode supported SOFCs were fabricated with varying GDC thickness. Special

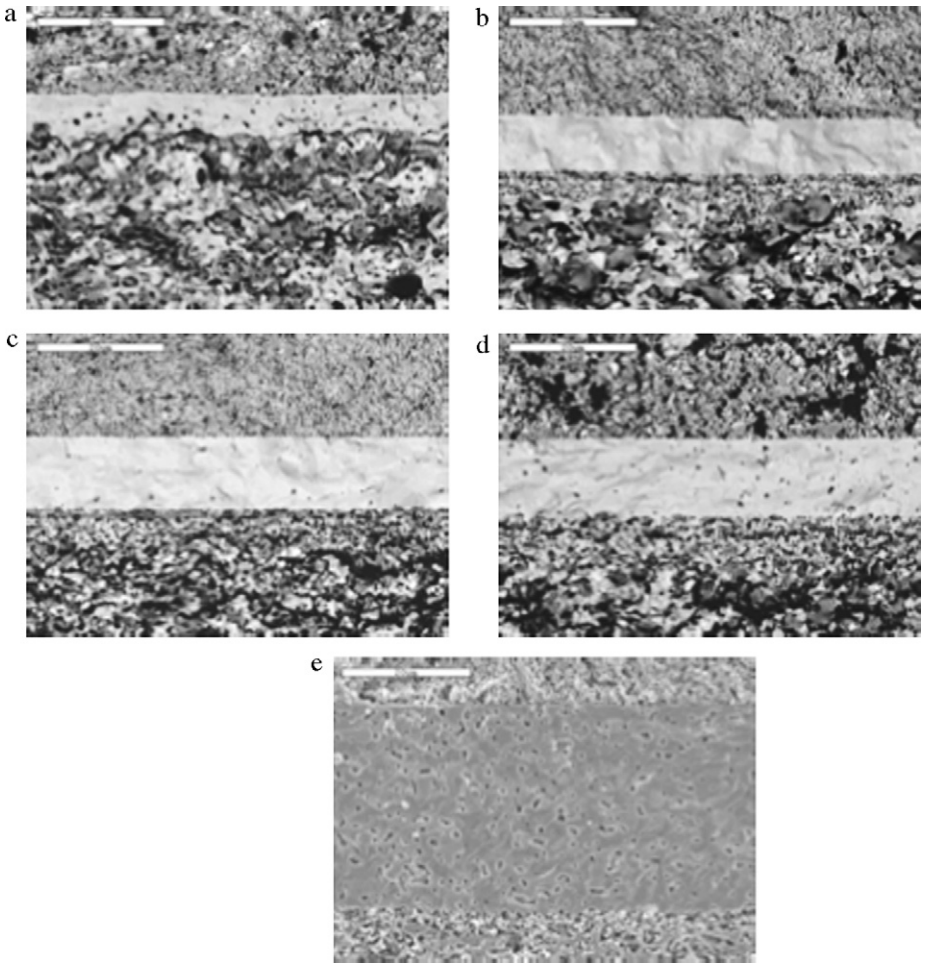

Fig. 2. SEMs of the cell cross-sections for electrolyte thicknesses of (a) 5.3 μm, (b) 9.4 μm, (c) 11.3 μm, (d) 12.6 μm and (e) 32.9 μm. In each figure, the top layer is LSCF-GDC cathode, the bottom layer is the Ni-GDC anode and the middle layer is the electrolyte. The anode functional layer (AFL) is not visible at these magnifications.

care was taken to fabricate the cells with high repeatability and steps were taken to minimize the variability between cells. Specifically, the anode supports were obtained from the same tape, while the anode functional layer (AFL) and cathode inks used were taken from the same batch.

3.1. Cell fabrication

NiO-GDC anode supports were prepared by tape-casting; using a mixture of NiO (Alfa Aesar) and GDC (Rhodia powder) with a 65:35 weight ratio. NiO and GDC powders were ball milled with Solsperse as a dispersant in a mixed toluene/ethyl alcohol solvent system for 24 h. Next, a plasticizer and a binder were added to the suspension and ball milled for another 24 h. A mixture of di-*n*-butyl phthalate (DBP) and polyethylene glycol (PEG), and polyvinyl butyral (PVB) were used as plasticizer, and binder, respectively. The slurry was then degassed in a vacuum chamber to prevent the formation of cracks or defects from air bubbles during the tape-casting process. Then a continuous NiO-GDC anode support tape was fabricated from the slurry on a Procast® tape casting system (DHI, Inc). After drying for 2 h at 100 °C, the NiO-GDC tape was punched into circular green bodies with 32 mm diameter and partially sintered at 900 °C for 2 h to get rid of residual organic binders and provide proper mechanical strength for the electrolyte deposition process.

NiO-GDC colloidal slurry, containing submicron size NiO (JT Baker®) and GDC (Rhodia powder) (65:35 wt %), was mixed with organic binders and coated on one side of anode support by spin coating to form an anode functional layer (AFL) for the SOFC. (The spin coater used was set at 1500 rpm for 15 s.) Subsequently, the anode substrates were pre-heated at 400 °C for the removal of the binders.

To fabricate dense GDC electrolytes, a GDC colloidal slurry was prepared and deposited by spin coating Rhodia® GDC powder was ball milled for 24 h with Solsperse® (dispersant) in ethanol. PVB (binder) and DBP (plasticizer) were added after the first ball-milling step and the solution was ball-milled for an additional 24 h. The spin coating was the same as for the AFL deposition. In order to control the thickness of GDC electrolyte, the spin coating process was repeated for each sample until the desired thickness was obtained. After deposition, samples were dried at room temperature for 10 h and the multilayered fuel cell structure was sintered at 1450 °C for 4 h in air.

$La_{0.6}Sr_{0.4}Co_{0.2}Fe_{0.8}O_{3-\delta}$ (LSCF)-GDC composite cathode were prepared and applied on the GDC electrolyte surface. Cathode inks were synthesized by mixing LSCF (Praxair®) and the GDC (Rhodia®) in a 50:50 weight% with organic binders. After mixing and grinding the cathode ink for 1 h, the ink was brush-painted onto the GDC electrolyte evenly. After applying the ink 3 times, the cathode was sintered at 1100 °C for 1 h. The active cathode area was ~0.4 cm^2. For current collection, Ag mesh and Pt wire were attached onto both electrode surfaces using Pt paste and then fired at 900 °C for 1 h.

3.2. Electrochemical characterization

Samples were loaded in a fuel cell testing set-up using 517-ceramabond sealant (Aremco®), 30 sccm of dry air and 30 sccm of

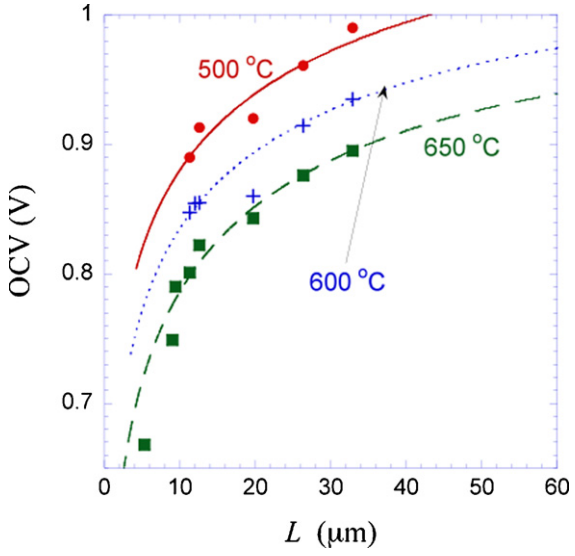

Fig. 3. Fit of the OCV model (Equation) to experimental data for open-circuit voltage (OCV) as a function of electrolyte thickness (L) for a Ni-GDC/GDC/LSCF-GDC cell.

wet hydrogen were supplied to the cathode and anode side, respectively. After reduction of anode for several hours, the open circuit voltage (OCV) and current–voltage (I–V) characteristics at various temperatures were obtained using a Solartron® 1287 potentiostat.

4. Results and discussion

Fig. 2 shows the SEMs of the cell cross-sections for various electrolyte thicknesses, from 5.3 μm to 32.9 μm. In each figure, the top layer is LSCF-GDC cathode, the bottom layer is the Ni-GDC anode and the middle layer is the electrolyte. The anode functional layer (AFL) is not visible at these magnifications.

The OCV model, Eqs. (10) and (11), was fitted to experimental data of open-circuit voltage as a function of electrolyte thickness for a Ni-GDC/GDC/LSCF-GDC cell, for three temperatures (500 °C, 600 °C and 650 °C), Fig. 3. The plot shows the model approximates the data quite well given the error inherent in the experiment. The results clearly show that as the electrolyte thickness decreases, so does the OCV for the cells. Moreover, the decrease in OCV per decrease in electrolyte thickness increases as L decreases, i.e., $\Delta OCV/\Delta L \propto 1/L$. Physically, this result suggests an exponential increase in the permeation flux as the electrolyte gets thinner. And, therefore, the reduction in ohmic resistance afforded by a thinner electrolyte is countered by a decrease in convertible energy (as indicated by the lower OCV).

The two parameters ($J_{ex,0}$ and $J_{ex,L}$) extracted from fitting the model, were plotted, Fig. 4, to verify Arrhenius behavior, since kinetic phenomena are normally parameterized by an activation energy. The excellent fits obtained from the plots (correlation coefficient, $R > 0.98$) confirm Arrhenius behavior, but, more significantly, they confirm the consistency of the OCV model. In practical terms, requiring that the extracted parameters conform to Arrhenius behavior increases their meaningfulness. The activation energies for the cathode and anode exchange current densities are comparable (1.1 eV for the anode and 0.94 eV for the cathode) and reasonable for these materials [24].

Fig. 5a shows the oxygen permeation flux through the GDC electrolyte (in open-circuit, i.e., zero current conditions) and OCV as a function of thickness, at 650 °C. Correspondingly, Fig. 5b shows a plot of OCV versus the permeation flux, at 650 °C. From the plots it is easy to see that as the electrolyte thickness decreases the oxygen permeation flux increases while the OCV decreases. Moreover,

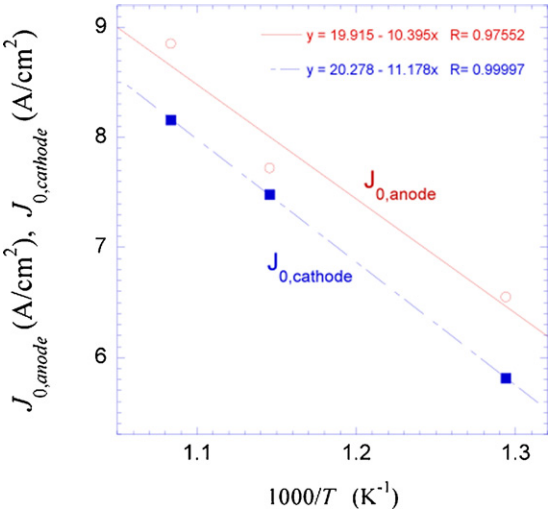

Fig. 4. Arrhenius plot of fitting parameters used to model the Ni-GDC/GDC/LSCF-GDC cell.

the plots show that if the electrolyte is made sufficiently thick theoretical/Nernst value for OCV is achievable; albeit at great cost to performance in closed-circuit ($J \neq 0$) conditions.

The continuum-level electrochemical model for SOFC performance, Eq. (14), was fitted to experimental data for a Ni-GDC/GDC/LSCF-GDC SOFC (with an anode functional layer) in Fig. 6a. Normally, the model uses three fitting parameters, K, α (i.e.,

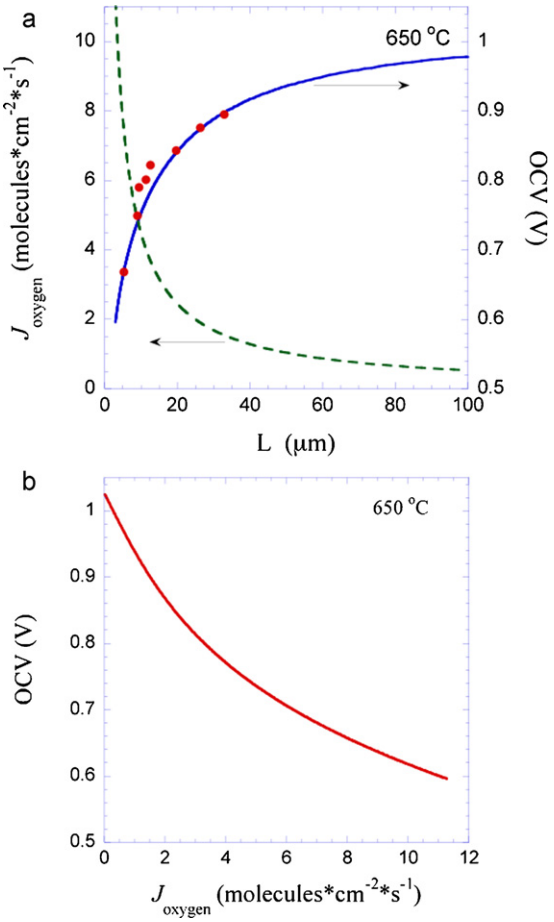

Fig. 5. (a) OCV and oxygen permeation flux as a function of electrolyte thickness at 650 °C; (b) OCV as a function of oxygen permeation flux at 650 °C.

$J_{ex,0}/J_{ex,L}$), and R_{elec} [1]. However, a K value of 4.64×10^{66} m^9 atm$^{1/2}$ was independently obtained from thermogravimetry experiments [25] on the same GDC powder used in the electrolyte and the electrodes. So with only two fitting parameters (α and R_{elec}) good agreement between model and data was obtained. This is a significant achievement considering contemporary performance models all use more (>5) fitting parameters and in some cases fit only about half the performance range (i.e., from open-circuit to maximum power density) [13,15,16].

The model returns a value of $\alpha = 1.19$ which means the effective exchange current densities for the anode is slightly better than the cathode for this cell. In addition, this value of α is almost identical to the value used to fit the OCV vs. L data, at 600 °C, in Fig. 3, which was $\alpha = J_{ex,0}/J_{ex,L} = 1.27$. The difference between the two values is 6.3%, which is well within the boundaries of reasonable experimental error. In addition, the model yields $R_{elec} = 0.001\ \Omega\ \text{cm}^2$, which is quite a small value, that demonstrates the effect of the AFL on lowering the effective ohmic resistance of the anode.

The parameters used in fitting the Ni-GDC/GDC/LSCF-GDC SOFC performance, in Fig. 6a, were then used to predict the dependence of the maximum power density (MPD) of that cell as a function of electrolyte thickness in Fig. 6b. The plot shows that (at MPD) though the ohmic overpotential (which is directly dependent on electrolyte thickness) decreases monotonically with decreasing electrolyte thickness, the electronic leakage current increases (exponentially) with decreasing electrolyte thickness. Consequently, as the electrolyte thickness decreases the MPD initially increases but when the leakage current becomes too great the MPD reverses course and begins decreasing, after passing through a local maximum. In other words, there exists an optimal electrolyte thickness for a mixed conducting electrolyte such as GDC. This concept is crucial, because it means that mixed conducting electrolytes should not be made arbitrarily thin. Reducing the electrolyte thickness increases the electronic leakage current and decreases the OCV, both of which mitigate and can even overwhelm the benefit of reduced ohmic overpotential.

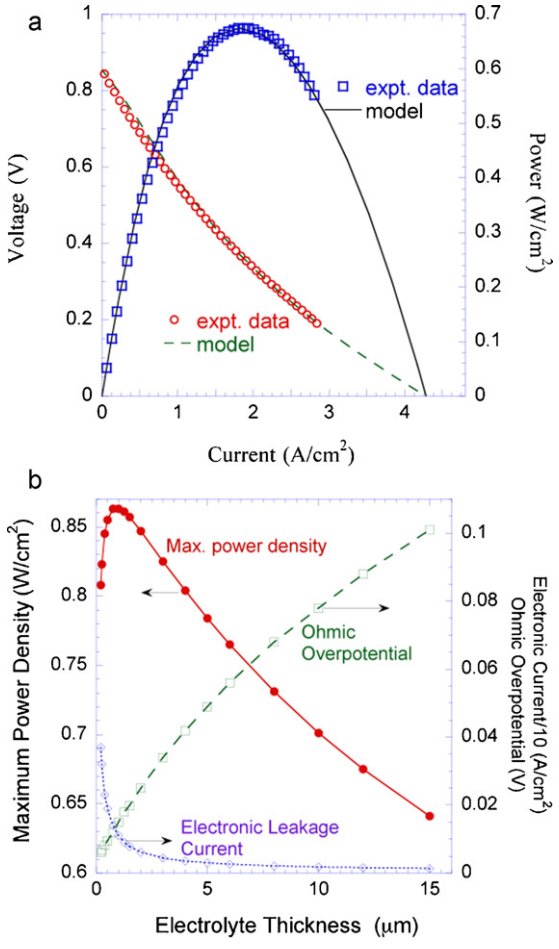

Fig. 6. (a) Model, Eq. (14), fitted to experimental data for current-voltage and current-power of a Ni-GDC/GDC/LSCF-GDC SOFC (with an anode functional layer) with a 12-μm thick electrolyte at 600 °C. (b) Projected maximum power density, electronic (leakage) current and ohmic overpotential as a function of electrolyte thickness predicted from model at 600 °C.

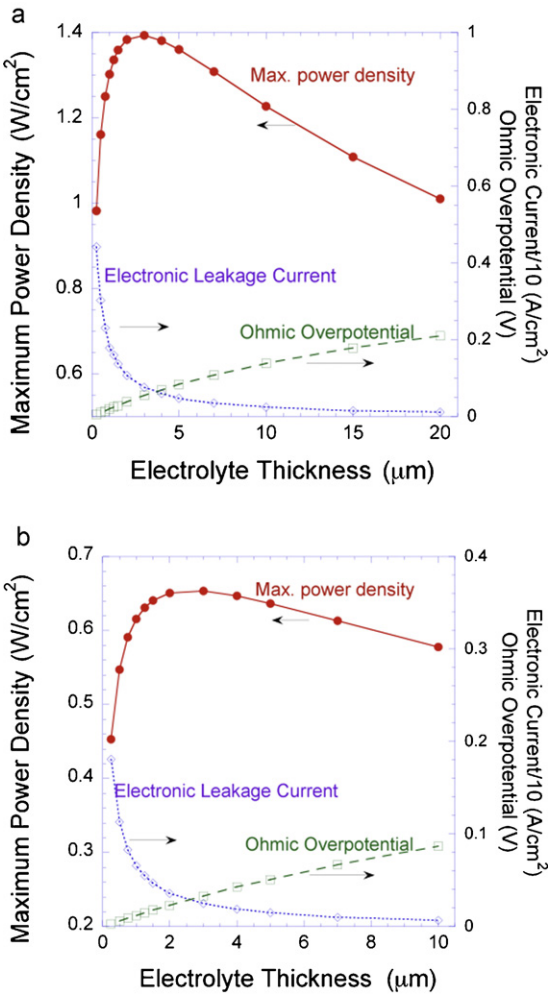

Fig. 7. Projected maximum power density, electronic (leakage) current and ohmic overpotential as a function of electrolyte thickness predicted from model at 600 °C for (a) Ni-SDC/SDC/BSCF [21] and (b) Ni-GDC/GDC/LSCF-GDC [22] cells.

Fig. 7 shows the MPD dependence on thickness generated for previously modeled SOFCs [21,22]. The basic trends obtained in Fig. 6b are also seen for these SOFCs. However, the shape of the curves were influenced by the electrode materials used for those SOFCs, which therefore have different values for α, $J_{0,ex}$, and K. These differences were discussed thoroughly in our earlier work [1].

5. Conclusions

The continuum-level electrochemical model for SOFC performance was applied to the dependence of open-circuit potential and maximum power density on electrolyte thickness for SOFCs with acceptor-doped ceria electrolytes.

Good fits of the model were obtained for experimental data for OCV versus thickness for different temperatures. Furthermore, the results showed that OCV decreases with decreasing L. This means

that for mixed conducting electrolytes the ideal SOFC electrolyte thickness is a compromise between the need to lower ohmic losses (thinner L) and the desire to maximize convertible energy (higher OCV). The fitting parameters were meaningful and conformed to expected Arrhenius behavior.

The continuum-level electrochemical model was fitted to SOFC performance (current–voltage, current–power) data using only two fitting parameters (down from three) because of the availability of accurate independent data for K from thermogravimetry. This is a significant improvement over competing models that use more fitting parameters (>5) thereby reducing the physical and statistical significance of each.

The SOFC performance parameters were then used in the model to predict the dependence of the maximum power density as a function of thickness for various SOFCs. The findings reveal that there is an optimal thickness at which the power density is the greatest. For thicknesses less than optimal the power density decreases due to high leakage current densities. Conversely, for thicknesses higher than optimal the power density is reduced due to growing ohmic losses.

In summary, the presence of electronic conductivity in mixed conducting electrolytes means that their thicknesses should not be chosen to be arbitrarily thin. Instead, their thickness must be part of the design strategy to maximize the SOFC performance requirements.

References

[1] K.L. Duncan, E.D. Wachsman, J. Electrochem. Soc. 156 (2009) B1030.
[2] B.C.H. Steele, J. Mater. Sci. 36 (2001) 1053.
[3] D. Brett, A. Atkinson, N. Brandon, Chem. Soc. Rev. 37 (2008) 1568.
[4] D.L. Meixner, D. Brengel, B. Henderson, J. Abrardo, M. Wilson, D. Taylor, R. Cutlerb, J. Electrochem. Soc. 149 (2002) D132.
[5] B.C.H. Steele, Curr. Opin. Solid State Mater. Sci. 1 (1996) 684.
[6] S.M. Haile, Acta Mater. 51 (2003) 5981.
[7] R.M. Ormerod, Chem. Soc. Rev. 32 (2003) 17.
[8] T. Matsui, T. Kosaka, M. Inaba, A. Mineshige, Z. Ogumi, Solid State Ionics 176 (2005) 663.
[9] I. Riess, Solid State Ionics 52 (1992) 127.
[10] M. Gödickemeier, L.J. Gauckler, J. Electrochem. Soc. 145 (1998) 414.
[11] M. Liu, J. Electrochem. Soc. 144 (1997) 1813.
[12] S. Yuan, U. Pal, J. Electrochem. Soc. 143 (1996) 3214.
[13] K.J. Yoon, W. Huang, G. Ye, S. Gopalan, U. Pal, D.A. Seccombe Jr., J. Electrochem. Soc. 154 (2007) B389.
[14] S.H. Chan, X.J. Chen, K.A. Khor, J. Power Sources 111 (2002) 320.
[15] R.T. Leah, N.P. Brandon, P. Aguiar, J. Power Sources 145 (2005) 336.
[16] B. Dalslet, P. Blennow, P. Hendriksen, N. Bonanos, D. Lybye, M. Mogensen, J. Solid State Electrochem. 10 (2006) 547.
[17] J. Newman, Electrochemical Systems, Prentice-Hall, New Jersey, 1991 (Chapters 2 and 11).
[18] H.J. Bouwmeester, P.J. Gellings, in: H.J. Bouwmeester, P.J. Gellings (Eds.), CRC Handbook of Solid State Electrochemistry, 1st ed., CRC Press, 1997 (Chapter 1).
[19] D. Pletcher, Instrumental Methods in Electrochemistry, Southampton Electrochemistry Group, Horwood, 2001.
[20] W. Weppner, in: H.J. Bouwmeester, P.J. Gellings (Eds.), CRC Handbook of Solid State Electrochemistry, 1st ed., CRC Press, 1997 (Chapter 9).
[21] Z. Shao, S.M. Haile, Nature 431 (2004) 170.
[22] Y.J. Leng, S.H. Chan, S.P. Jiang, K.A. Khor, Solid State Ionics 170 (2004) 9.
[23] J. Ahn, H. Yoon, E Wachsman, Solid State Ionic Dev. V: ECS Trans. 11 (2008) 99.
[24] J. Liu, A.C. Co, S. Paulson, V.I. Birss, Solid State Ionics 177 (2006) 377.
[25] S.R. Bishop, K.L. Duncan, E.D. Wachsman, Electrochim. Acta 54 (2009) 1436.